Direct Laser Writing of Four-Dimensional Structural Color Microactuators Using a Photonic Photoresist

Marc del Pozo [1], Colm Delaney [2], Cees W.M. Bastiaansen [1,3], Dermot Diamond [4],

*Albert P.H.J. Schenning [1 *], and Larisa Florea [2 *]*

[1] Stimuli-responsive Functional Materials and Devices, Department of Chemical Engineering, Eindhoven University of Technology, P.O. Box 513, 5600 MB Eindhoven, The Netherlands.

[2] School of Chemistry and AMBER, the SFI Research Centre for Advanced Materials and BioEngineering Research, Trinity College Dublin, the University of Dublin, College Green, Dublin 2, Ireland.

[3] School of Engineering and Materials Science, Queen Mary University of London, Mile End Road, London E1 4NS, UK.

[4] Insight Centre for Data Analytics, National Centre for Sensor Research, School of Chemical Sciences, Dublin City University, Glasnevin, Dublin 9, Ireland.

* Corresponding author´s e-mail: a.p.h.j.schenning@tue.nl and floreal@tcd.ie

ABSTRACT

With the advent of direct laser writing (DLW) using two-photon polymerization (TPP) the generation of high resolution three-dimensional (3D) microstructures has increased dramatically. However, the development of stimuli-responsive photoresists to create four-dimensional (4D) microstructures, remains a challenge. Herein, we present a supramolecular cholesteric liquid crystalline (CLC) photonic-photoresist for the fabrication of 4D photonic micro-actuators, such as pillars, flowers, and butterflies, with sub-micron resolution. These micron-sized features display structural color and shape changes triggered by variation of humidity or temperature. These findings serve as a roadmap for the design and creation of high-resolution 4D photonic micro-actuators.
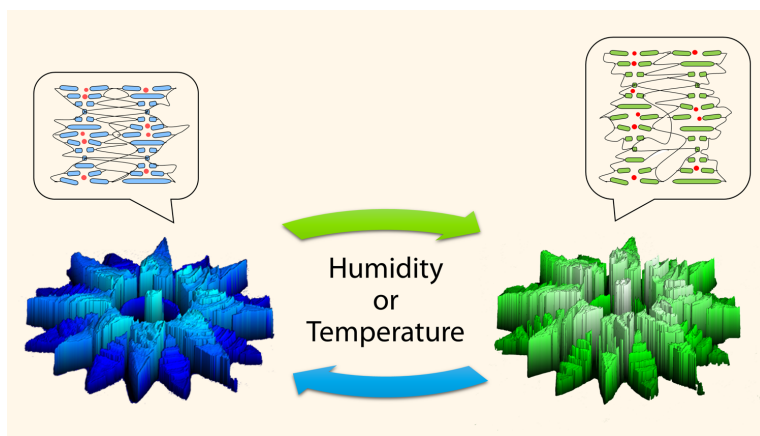
KEYWORDS: *direct laser writing, two-photon polymerization, cholesteric liquid crystal networks, photonic-photoresist, dynamic structural color, 4D photonic micro-actuators*.

2

Over the last decade, the availability of commercial two-photon polymerization direct laser writing (TPP-DLW) systems has resulted in a plethora of high-resolution three-dimensional (3D) microstructures.[1,2] Owed to the freedom of design, TPP-DLW is of special interest in fields such as microfluidics,[3] microelectromechanical systems (MEMS),[4] biotechnology,[5,6] surface modification,[7,8] microrobots,[9,10] anti-counterfeiting,[11,12] and photonics[13–16] in which micron-sized features are required. To date, micro-actuators that respond to external stimuli have been fabricated using TPP-DLW from hydrogels of low crosslinking density,[17–20] polymerizable ionic liquids (PIL),[21] and liquid crystals (LC)[22–26] photoresists. However, low crosslink density networks are hampered by swelling in the surrounding photoresist[27] which affects resolution.[28] Therefore, it remains a challenge to create micron-sized four-dimensional (4D) photonic micro-actuators that would be appealing for the aforementioned fields to sense external stimuli such as temperature, light or other environmental stimuli and act by changing their color and shape in response.[29]

Herein we report a photonic-photoresist, based on supramolecular cholesteric liquid crystals (CLC), for the generation of stimuli-responsive photonic micro-actuators *via* TPP-DLW. CLC networks exhibit a self-organized helical photonic structure that can selectively reflect light (**Figure 1**).[30] These networks can respond to a stimulus which triggers a shift in the reflection band, as a result of an anisotropic shape change of the helix.[31,32] To date, CLCs have been used in combination with TPP-DLW to investigate the effect of the surrounding monomer on the pitch of the polymerized CLC network[27,33,34] or to fabricate a stable uniform lying helix state,[35] but have not yet been explored for the fabrication of 4D photonic micro-actuators. The photonic-photoresist presented here consists of a CLC monomer mixture comprising reactive mesogenic monomers, a chiral dopant, mono-functional acrylate, and carboxylic acid mesogens (**Figure 1a**). The inclusion of carboxylic acid functionalized molecules enables the formation of hydrogen bonds which act as

supramolecular crosslinkers during the TPP-DLW, thereby enabling sub-micron resolution. After fabrication, base treatment can then be used to cleave the hydrogen bonds, thereby reducing the crosslinking density and rendering a stimuli-responsive network. We demonstrate that the marriage of stimuli-responsive self-ordering materials with TPP-DLW enables the fabrication of a range of dual-responsive 3D microstructures, which can respond to variations in humidity and temperature through modulation of their shape and color. We present full structural characterization of these 4D photonic micro-actuators and a comprehensive study on their structural and optical responses.

RESULTS AND DISCUSSION

The photonic-photoresist reported here is based on a hydrogen bonded CLC mixture which can be polymerized into coatings to demonstrate structural color and shape changes.[32,36] Optimization of the photonic-photoresist composition, to enable room temperature fabrication, yielded a LC mixture comprising the compounds in **Figure 1a**. The optimized photonic-photoresist has an isotropic to chiral nematic phase at ~48 °C that is stable at room temperature for several hours without crystallizing (**Figure S1**). The di-functional mesogenic acrylates **1-2** act as chemical crosslinkers to ensure that a network is obtained during the TPP-DLW fabrication process. The mono-functional mesogenic acrylates **3-4** add flexibility to the network. The mono-functional mesogenic carboxylic acids **5-8** act as supramolecular hydrogen bonded crosslinkers during the TPP-DLW fabrication. After polymerization, the hydrogen bonds can be cleaved *via* base treatment, by exposing the structures to 1M KOH for 1 minute. This gives flexibility and humidity-responsiveness to the network due to the creation of a charged, hygroscopic polymer. The chiral dopant **9** (optimized at 2.3 mol%) induces a helical organization in the nematic LC mixture to achieve a photonic-photoresist, with a reflection band centered at 400 nm (**Figure S2**). Lastly, 0.8 mol% of Irgacure 819 photoinitiator was added. This photoinitiator has been previously employed as a two-photon free-radical initiator for acrylate-based resins in TPP-DLW.[37–41] To ensure covalent attachment of the microstructures to the substrate, the glass surface was treated with 3-(trimethoxysilyl)propyl acrylate. The fabrication of photonic micro-actuators *via* TPP-DLW and subsequent activation are depicted in **Figure 1b**.
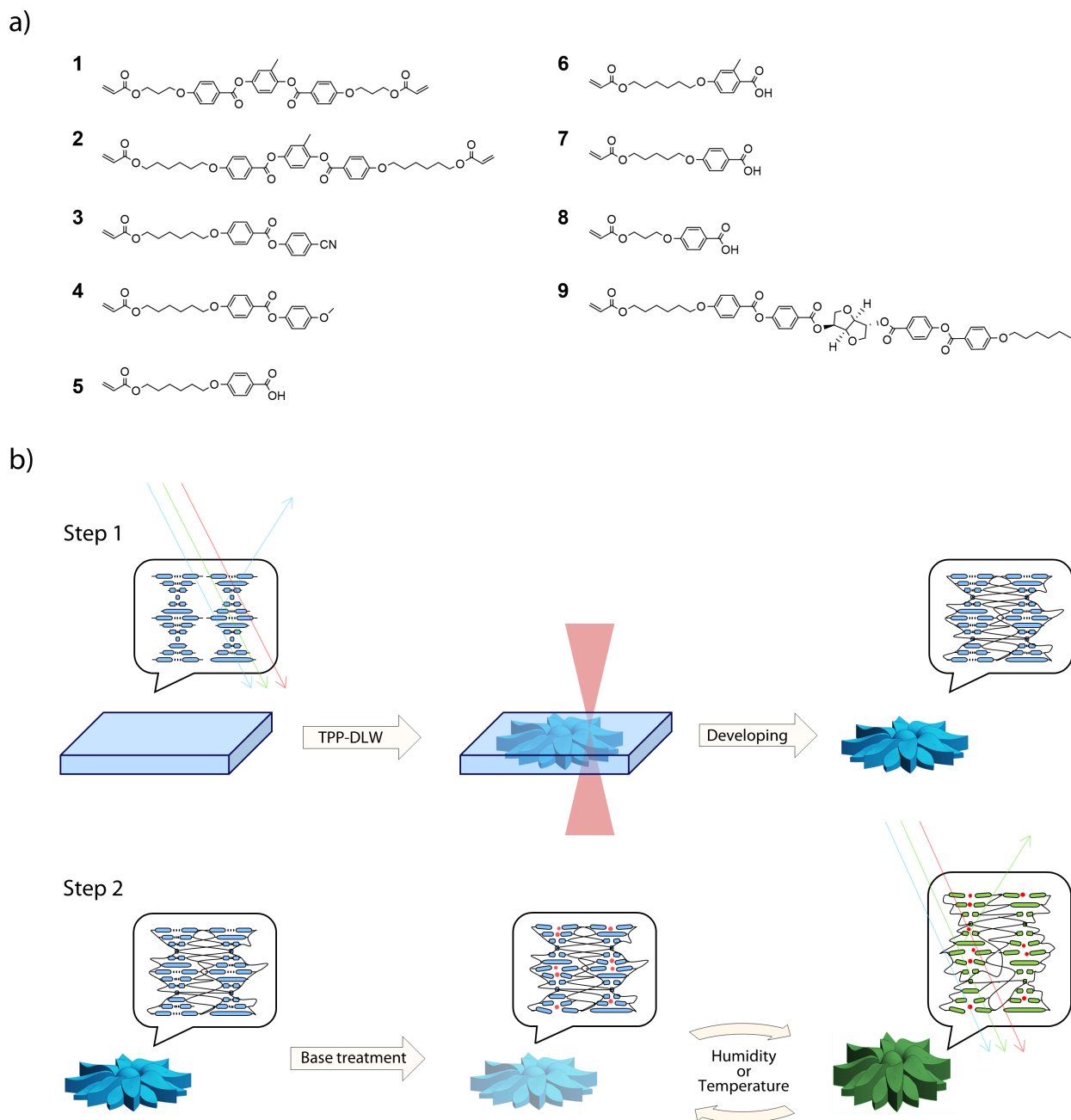
a)

b)

Figure 1. a) Overview of the reactive mesogenic monomers used to prepare the photonic-photoresist. b) Schematic of the fabrication (Step 1) and structure activation (Step 2), to obtain 4D photonic micro-actuators. Red spheres represent the potassium cations present after base treatment.

To initially test and optimize the DLW set-up, arrays of micron-sized square pillars were fabricated, **Figure 2**. Optimized printing parameters yielded writing speeds between 5000 μm·s^{-1}-10000 μm·s^{-1}, with laser powers between 40-45%. To ensure complete attachment to the functionalized surface, fabrication of the structures started at -0.5 μm from the glass/photonic-photoresist interface and any minor mismatch between the structure height and computer assisted design (CAD) can be attributed to this. After removing the unreacted monomer, the pillars show a blue reflection which confirms the preservation of cholesteric alignment, as shown in **Figure 2** and **Figure S3**. Visualization of the photonic character of the objects is enhanced through the use of crossed linear polarizers (**Figure S4**). Polymerization was confirmed *via* confocal Raman
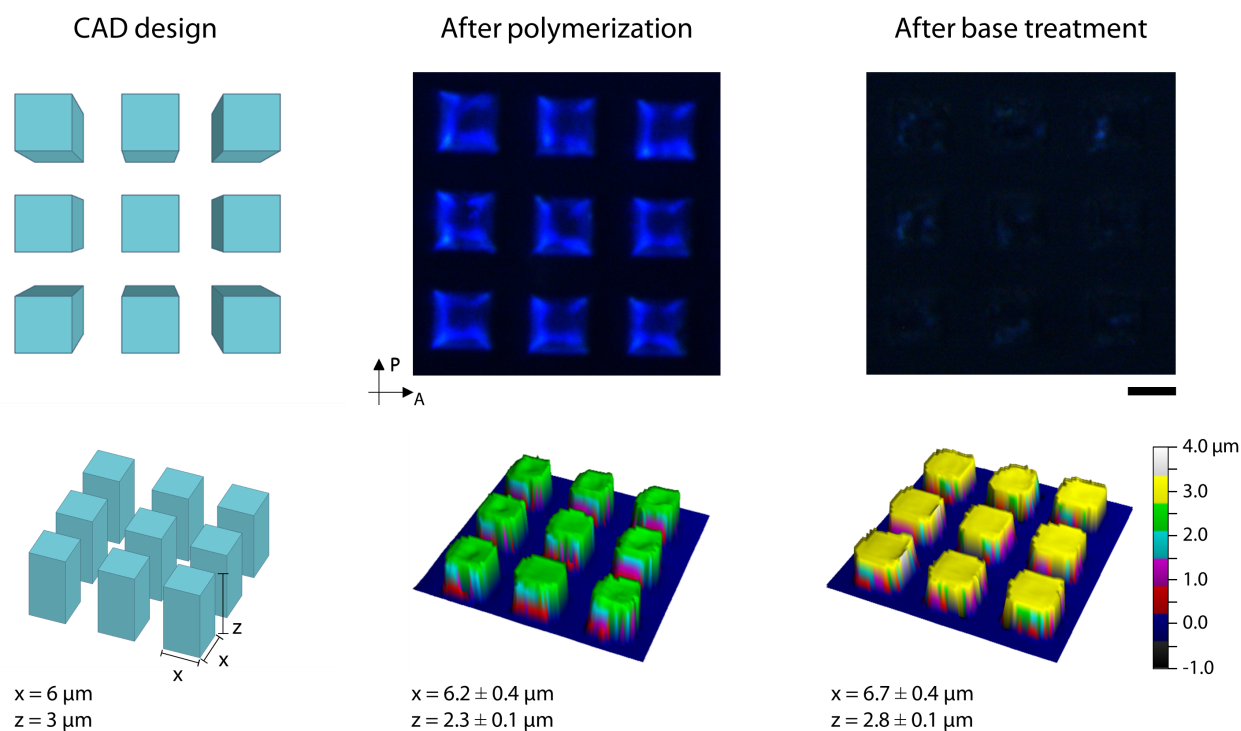

CAD design	After polymerization	After base treatment
x = 6 μm	x = 6.2 ± 0.4 μm	x = 6.7 ± 0.4 μm
z = 3 μm	z = 2.3 ± 0.1 μm	z = 2.8 ± 0.1 μm

Figure 2. Structural and optical characterization of an array of pillars after polymerization and after base treatment. Top-crossed polarized micrographs; bottom-3D profiles of the array of pillars. The scale bar represents 10 μm.

spectroscopy, by observing the reduction of the peak corresponding to the double bond stretch of the acrylate group at 1635 cm^{-1} (**Figure S5**). The shape of the pillars was characterized using an optical profiling system. The CAD design comprised pillars of 6 μm width and a height of 3 μm in a square lattice. The fabricated pillars showed an average width of 6.2 ± 0.4 μm, and an average height of 2.3 ± 0.1 μm. Such high fidelity between the fabricated object and design file indicates that only minimal swelling occurred during the TPP-DLW process; most likely due to the highly effective supramolecular crosslinking density achieved during fabrication.

Subsequent base treatment of the pillars served to cleave the hydrogen bonds between molecules **5-8**; as verified *via* confocal Raman spectroscopy by observing the reduction of the carboxylic acid peaks at 1647 cm^{-1} and 1280 cm^{-1} and the appearance of the carboxylic salt peak at 1395 cm^{-1} (**Figure S5**). This treatment results in a charged hygroscopic photonic polymer which is sensitive to changes in humidity and temperature.[36,42] **Figure 2** shows the pillars before (middle) and after the base treatment (right). Firstly, the micrograph indicates that the activation step has reduced the intensity of the reflection band, which is a phenomenon also observed in a homogeneous coatings made with the same photonic-photoresist **(Figure S2)** that is attributed to the loss of molecular order due to the cleavage of the hydrogens bonds.[36,42] Secondly, the dimensions of the pillars appear to be slightly bigger than prior to the activation step, showing an average width of 6.7 ± 0.4 μm with an average height of 2.8 ± 0.1 μm. This difference can be explained due to the fact that the structures are now responsive to humidity changes (*vide infra*).

Photonic microstructures were then fabricated to explore the possibilities of making high resolution photonic 3D constructs (**Figure 3**). A flower (**Figure 3a)**, a butterfly (**Figure 3b**, **Figure S6**) and the pattern of the wing of the *Papilio paris* butterfly (**Figure 3c)** were fabricated. In the micrograph of the flower, the tiered layers of the structure can be easily observed. In this instance,
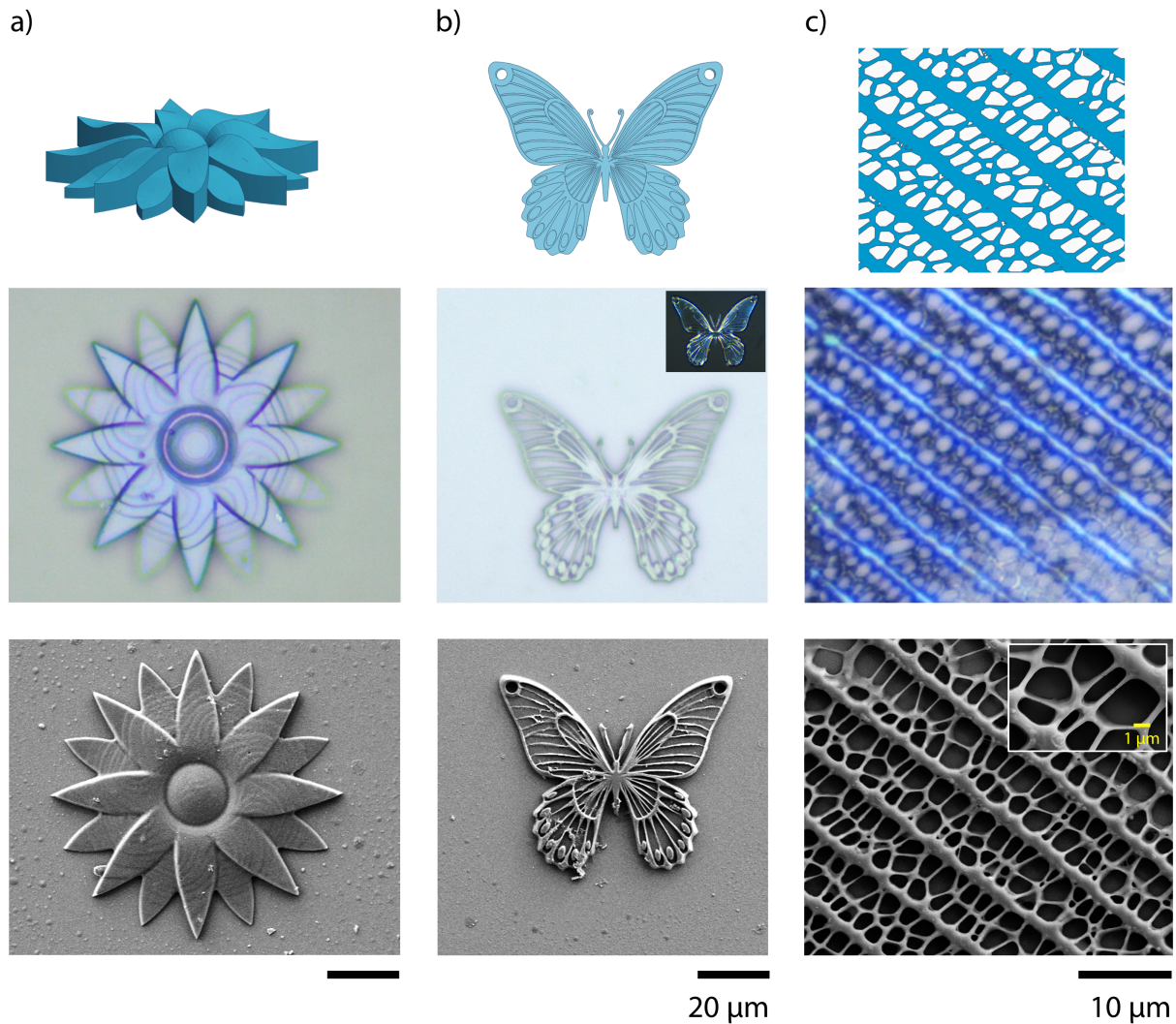
Figure 3. Photonic 3D microstructures. From top to bottom, the CAD designs of the structures, optical microscopy and SEM images before base treatment of (a) a flower, (b) a butterfly, and (c) the pattern of the wing of the *Papilio paris* butterfly. The inset in b) is a crossed linear polarized micrograph of the butterfly, used to enhance observation of the reflected color.

a slice thickness of 0.5 μm was used to fabricate the 6 μm tall flower. In the other structures such layers are not clearly visible due to their geometry and decreased slice thickness. In all cases, the structures displayed a blue color after fabrication, confirming preservation of the photonic

structure within the polymer and showing good fidelity with the computer design, even after base treatment (**Figure S7**). The biomimetic pattern, shown in **Figure 3c**, serves to demonstrate the capabilities of the photonic-photoresist, when used with TTP-DLW, to produce high-resolution nanometer features. Additional fabrication studies, shown in **Figures S8-S10**, confirm that feature sizes below 200 nm can be reproducibly fabricated using the methods outlined herein.

It is worth noting that for the butterfly, shown in **Figure 3b**, the amount of light reflected is notably less than other structures owed to the small height of features. To efficiently reflect light, a minimum height needs to be achieved, which can be calculated using the following equation:

$$\lambda = n \cdot P \cdot \cos(\theta) \tag{1}$$

in which λ is the center of the reflection band, n is the refractive index, P is the pitch size, which represents a full rotation of the molecules, and θ is the incident angle.[30] Taking the center of the reflection band to be at 400 nm (**Figure S2**), an incident angle of 90° and a refractive index of 1.5, the calculated pitch size is 266 nm. As at least ten pitches are required to efficiently reflect light, the minimum feature height to reflect light is 2.66 μm, as clearly observed in **Figure S11**. For this reason, reflected color of features with heights in this range can only be observed between polarizers, as seen in **Figure 3b** (inset).

The response of CLC networks, outlined in **Equation 1**, shows that a change in pitch results in a shift of the reflection band, with an increase in pitch resulting in a relative red shift, and a decrease resulting in a blue shift. A detailed characterization of the flower shown in **Figure 3** was conducted by an optical profiling system, to characterize shape change (**Figure 4**) and by an optical microscope to quantify color change (**Figure 5**). **Figure 4a** shows the height increase of the flower across a range of temperatures and humidity values; the corresponding dew points can be found in

Figure S12. The control of humidity was achieved through the use of a custom-built humidity

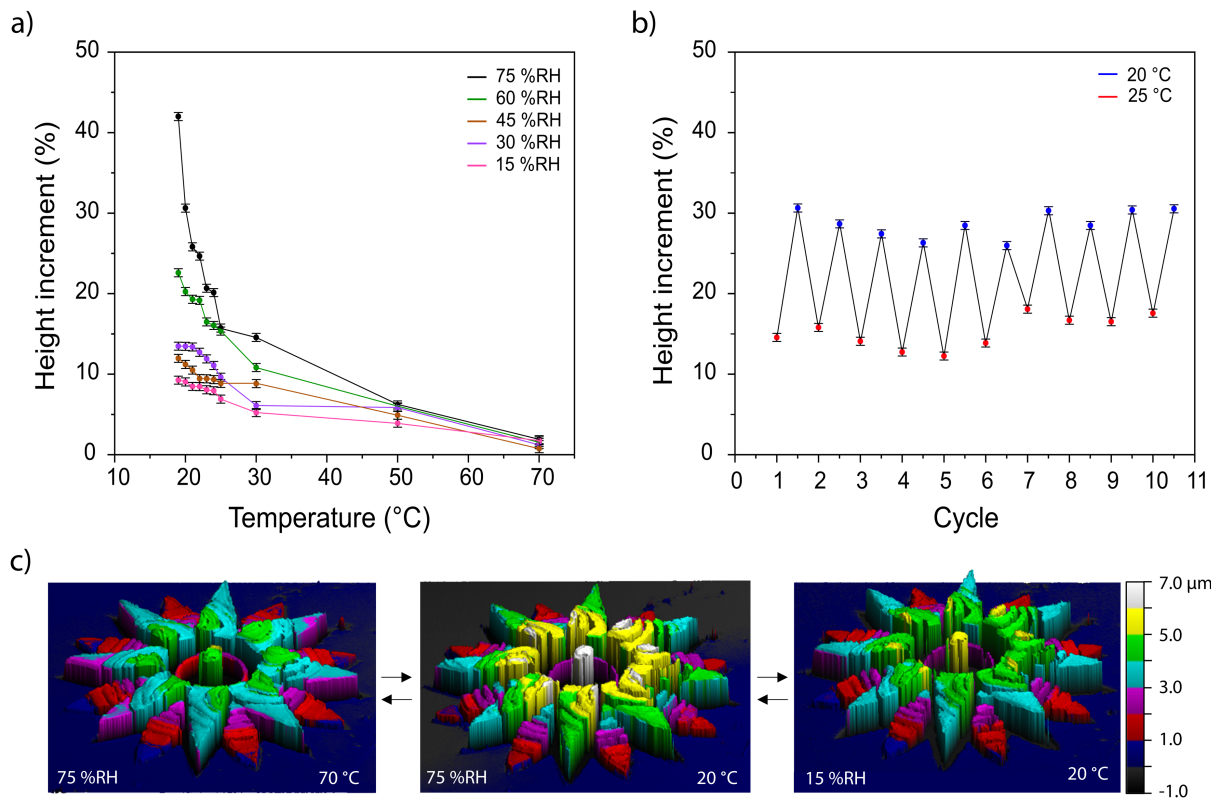chamber which encased the sample and the microscope objective. At 75 percent relative humidity

Figure 4. Characterization of the actuation of a flower at different atmospheric conditions and

temperatures. a) Height changes of the flower over a ranges of different temperature and humidity

values. b) Increment of the flower height over ten cycles, going from 25 °C to 20 °C, at 75 ± 2

%RH. For both a) and b), the percentage of height increment is obtained by averaging the values

of the top of the flower and comparing them to the height of the flower before base treatment. For

all measurements, the flower was held for 5 min after reaching the desired conditions before

recording its height. Error bars represent standard deviations for N=3 measurements. c) 3D profiles

of the flower which depict direct (triggered by humidity) or indirect (triggered by temperature)

actuation.

(%RH), as the temperature of the structure reached the dew point (18 °C), the height increased dramatically and reached an increase of 42 % at 19 °C. This trend was also observed for the 60 %RH measurements showing a maximum height increase of 22 % at 19 °C. However, at 15 %RH the increment was less steep, owed to a larger temperature deviation from the calculated dew point (-5 °C). Upon heating, water was removed from the flower, which resulted in a decrease in height. At 70 °C, regardless of the humidity, the structure showed no discernible change in height. **Figure 4b** demonstrates the reversibility of the response at 75 %RH, over ten cycles, between 25 °C (12-18 % expansion) and 20 °C (25-30 % expansion). It is known that the shape change of the structures is related to the charged hygroscopic polymer network obtained after base treatment which, in the presence of water vapors, results in a significant uniform expansion of the polymer network,[30,36] which occurs perpendicular to the glass substrate. **Figure 4c** shows the dynamic response in the flower's height when changes in humidity or in temperature occur. When the relative humidity is varied, the amount of water vapor in air changes (**Table S1**) and accordingly the flower expands or contracts. This may also be achieved by modulating the temperature of the structure. As temperature dictates the rate of water evaporation, increasing temperature results in contraction of the structure. Conversely, decreasing temperature close to the dew point results in expansion. This enables actuation of the structures directly (*via* humidity changes) and indirectly (*via* temperature changes).

The controlled expansion of the micro-actuators *via* temperature or humidity triggers changes in the pitch of the ordered CLC, thereby leading to variations in the reflection band (**Figure 5a**). **Figure 5b** shows the color change of the structure achieved by varying temperature at constant 75%RH. The data points were obtained from the corresponding polarized micrographs, **Figure S13**, following a previously reported procedure.[43] Upon decreasing the temperature, a gradual and
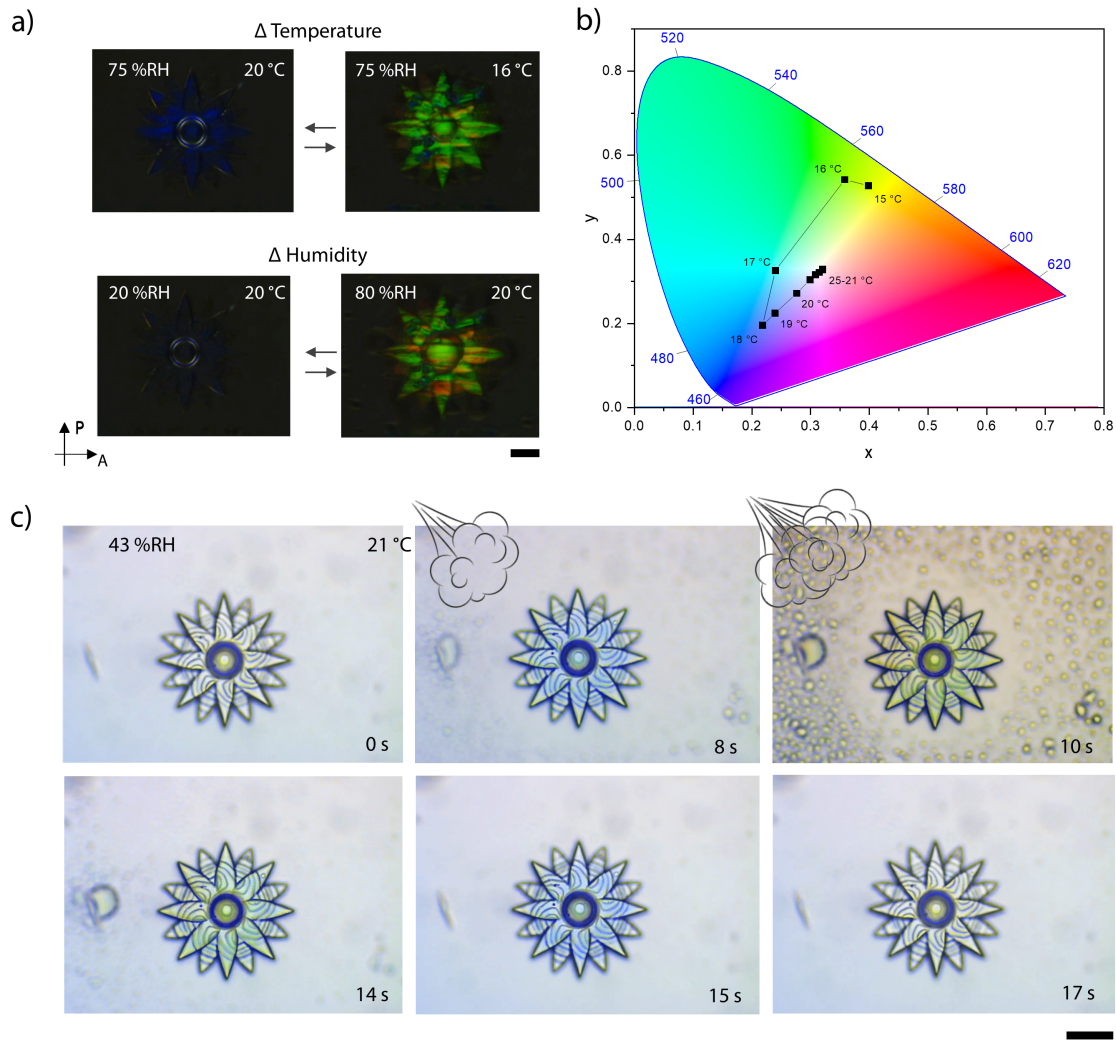
Figure 5. Characterization of the optical response of the microflower; a) Crossed polarized micrographs of the flower showing the direct (triggered by humidity), or indirect (triggered by temperature), induced color changes. b) Chromaticity diagram (standard CIE 1931) showing the color changes of the flower over a range of temperatures, at a constant 75 %RH. The data points are obtained from the corresponding crossed polarized micrographs that can be found in the supporting information. c) A sequence of micrographs that display the optical response of the flower upon exposure to breath (top row) and after (bottom row). All scale bars represent 20 μm.

linear response of color change from colorless to light blue was observed. However, it was not until below the dew point (18 °C), that the flower showed its most spectacular color change, from light blue to bright green, corresponding to the increased water absorption of the network.[36]

The dual-response of this type of 4D photonic micro-actuators can be seen in **Figure 5c** and in **Video V1**. When breathing on top of the flower, it displayed the same response as observed in **Figure 5b**, but this time much faster and stronger due to the steeper and higher change in humidity. As a result, the flower changes from transparent to blue in ~ 8 s and from blue to green within ~ 4 s and then recovers its initial state within ~ 3 s, **Figure S14**. This demonstrates the ability to exploit a fast visual response, which can be attributed to the miniaturization of the system when compared with analogous macro-sized systems.[32,36] This behavior shows how, for example, the system presented herein is attractive for the fabrication of 4D photonic micro-actuators in which the synergistic photonic response can act as a visual probe for shape change or for the generation of fast response anti-counterfeiting features. Furthermore, the incorporation of structural color in microstructures can be used to enhance their visualization and enable real-time interrogation, as recently shown for microrobots.[44]

CONCLUSIONS

In conclusion, through the development of a supramolecular photonic-photoresist, high resolution 4D photonic micro-actuators were fabricated *via* TPP-DLW. These structures showed a dual-response to changes in humidity (directly) and temperature (indirectly). The shape change, up to 42 % at 75 %RH, is attributed to the hygroscopic character of the polymer network. The controlled expansion of the micro-actuators at different temperature and humidity values results in a

corresponding color change, owed to modulation of the nanoscale CLC pitch in the ordered network. A measurable intrinsic color change could be beneficial in MEMS or in microrobots to enable facile real-time verification of their status.

METHODS

Materials and Reagents. 2-methyl-1,4-phenylene bis(4-(3-(acryloyloxy)propoxy)benzoate) (**1**), 2-methyl-1,4-phenylene bis(4-((6-(acryloyloxy)hexyl)oxy)benzoate) (**2**), 4-cyanophenyl 4-((6-(acryloyloxy)hexyl)oxy)benzoate (**3**), and 4-methoxyphenyl 4-((6-(acryloyloxy)hexyl)oxy)benzoate (**4**) were purchased from Merck. 4-((6-(acryloyloxy)hexyl)oxy)benzoic acid (**5**) was supplied by Ambeed. 4-((6-(acryloyloxy)hexyl)oxy)-2-methylbenzoic acid (**6**), 4-((5-(acryloyloxy)pentyl)oxy)benzoic acid (**7**), and 4-(3-(acryloyloxy)propoxy)benzoic acid (**8**) were provided by Synthon. (3R,3aS,6S,6aS)-6-((4-((4-((6-(acryloyloxy)hexyl)oxy)benzoyl)oxy)benzoyl)oxy)hexahydrofuro[3,2-b]furan-3-yl 4-((4-(hexyloxy)benzoyl)oxy)benzoate (**9**) was synthesized as previously reported.[45] Irgacure 819 was purchased from Ciba Specialty and 3-(trimethoxysilyl)propyl methacrylate from Sigma Aldrich. Potassium hydroxide pellets (85 %) was obtained from Alfa Aesar. All solvents were purchased from Biosolve.

Photonic-photoresist Preparation. The CLC monomer mixture consisted of 3.4 mol % **1**, 3.1 mol % **2**, 12.4 mol % **3**, 11.0 mol % **4**, 15.3 mol % **5**, 29.2 mol % **6**, 10.7 mol % **7**, 11.9 mol % **8**, 2.3 mol % **9**, and 0.8 mol % Irgacure 819. All components were dissolved in tetrahydrofuran. Solvent was removed at 80 °C overnight. Characterization of the resulting CLC mixture can be found in the Supplementary Information.

Cell Preparation. High precision microscope cover glasses (22x22 mm^2, thickness 170 ± 5 μm; No 1.5; from Marienfeld) were cleaned by sonication for 20 min in acetone. For functionalization, slides were treated in a UV-ozone photoreactor (Ultra Violet Products, PR-100) for 20 min to activate the surface and were immediately functionalized with methacrylate groups by spin coating (3000 rpm, 45 s) a 3-(trimethoxysilyl)propyl methacrylate solution (1 vol. % solution in a 1:1 water-isopropanol mixture) followed by a curing step of 10 min at 100 °C. Following this, the functionalized slide was attached to a second, unfunctionalized slide, using a 50 μm thick double adhesive tape spacer, to form a simple cell assembly.

Computer Design of the 3D Structures. All structures were fabricated based on a computer design. The design of the structures was custom-made by the authors using SketchUp or adapted from files licensed under the Creative Commons Attribution 4.0 International license and available at www.thingiverse.com. These can be downloaded from the creators at the respective links: www.thingiverse.com/thing:2500769 for the flower, www.thingiverse.com/thing:816098/files for the butterfly. The files were modified using DeScribe 2.4.4 software to choose the slicing (0.2-0.5 μm) and hatching (0.2 μm) values.

Direct Laser Writing. The cell was filled by capillarity with the CLC mixture at room temperature. The filling resulted in an aligned CLC. Localized TTP was conducted in a commercial DLW workstation (Photonic Professional, Nanoscribe GmbH) equipped with a 170-mW femtosecond solid-state laser (λ = 780 nm) that delivers 120-fs pulses with an 80 MHz ± 1 MHz repetition rate. At a power scaling of 1, the average laser output is 50 mW. The laser beam was focused with a 63x oil objective (NA = 1.4; WD = 190 μm; Zeiss; Plan Apochromat) into the filled cell. The sample movement was controlled by a piezo translation stage in the z axis and by a galvo stage in the *x*- and *y*-axis. The fabrication of the 3D microstructures was performed at different

laser powers (40 % - 45 %) and scan speeds (5000 μm s^{-1} – 10000 μm s^{-1}) depending on the structure's geometry, and hatching, and slicing values. Structure fabrication was initiated 0.5 μm below the automatically detected glass/photonic-photoresist interface. After TPP-DLW, the structures were washed in warm isopropanol until all the unreacted monomer had dissolved. The cell was then opened and the functionalized glass rinsed with isopropanol and air-dried. The activation of the structures was performed by placing a drop of 1M KOH solution on top of the structures for 1 min. The basic solution was rinsed with water and the structures were then dried by heating at 70 °C for 10 min using a hot plate.

Characterization. Micrographs were recorded on a Leica DM2700M polarized optical microscope equipped with a Leica MC170 HD camera. The video was recorded using OBS Studio software. All structures were visualized in bright field and in reflection mode. The 3D profiles of the structures were obtained using an optical profiling system (Zoomsurf 3D; Fogale nanotech). To measure the height and color changes at different humidity and temperature, both the microscope and the profiling system were equipped with a transparent custom-built humidity chamber in which the internal humidity and air temperature were controlled manually and monitored with a sensor (SHT3x, Sensirion) and the temperature of substrate controlled with a Linkam TMS 600 hot-stage. The specific humidity values, corresponding to the different relative humidity values and air temperatures, can be found in **Table S1**. Electron micrographs were recorded using a Zeiss ULTRA Plus Scanning Electron Microscope. The structures were coated, prior to imaging, with a 10 nm Au-Pd layer using a Cressington Sputter Coater 208HR and a 57 x 0.1 mm Au-Pd target (TED PELLA INC.).

Image Analysis. The crossed polarized micrographs of microflower at different temperatures and constant humidity (**Figure S13**) were acquired by keeping constant the camera acquisition

settings to avoid false color change. The images were analyzed without any modification. First, the average RGB values from the images were obtained using Image J software. Then, the RGB values were transformed to (x,y) values to be plotted in a chromaticity diagram (standard CIE 1931) as previously reported.[43]

ASSOCIATED CONTENT

Supporting Information:

This material is available free of charge *via* the internet at http://pubs.asc.org

> DSC measurements and UV-Vis spectrum of the photonic-photoresist; further characterization on the microstructure that includes extra micrographs, SEM images, and 3D profiles either before and/or after base treatment; theory on how the visualization of the optical properties is obtained by using crossed linear polarizers; confocal Raman spectroscopy; micrographs showing the influence of structure height on intensity; dew point calculations; optical response of a microflower in response to temperature changes; time-dependent color change; calculation on the specific humidity based on relative humidity values; movie showing the optical response of a microflower to breath.

AUTHOR INFORMATION

Corresponding Author

Larisa Florea: floreal@tcd.ie

Albert P.H.J. Schenning: a.p.h.j.schenning@tue.nl

Author Contributions

The manuscript was written through contributions of all authors. All authors have given approval to the final version of the manuscript.

REFERENCES

(1)   Zhang, Y. L.; Chen, Q. D.; Xia, H.; Sun, H. B. Designable 3D Nanofabrication by Femtosecond Laser Direct Writing. *Nano Today* **2010**, *5*, 435–448.

(2)   Malinauskas, M.; Farsari, M.; Piskarskas, A.; Juodkazis, S. Ultrafast Laser Nanostructuring of Photopolymers: A Decade of Advances. *Phys. Rep.* **2013**, *533*, 1–31.

(3)   Sugioka, K.; Xu, J.; Wu, D.; Hanada, Y.; Wang, Z.; Cheng, Y.; Midorikawa, K. Femtosecond Laser 3D Micromachining: A Powerful Tool for the Fabrication of Microfluidic, Optofluidic, and Electrofluidic Devices Based on Glass. *Lab Chip* **2014**, *14*, 3447–3458.

(4)   Jayne, R. K.; Stark, T. J.; Reeves, J. B.; Bishop, D. J.; White, A. E. Dynamic Actuation of Soft 3D Micromechanical Structures Using Micro-Electromechanical Systems (MEMS). *Adv. Mater. Technol.* **2018**, *3*, 1–6.

(5)   Marino, A.; Desii, A.; Pellegrino, M.; Pellegrini, M.; Filippeschi, C.; Mazzolai, B.; Mattoli, V.; Ciofani, G. Nanostructured Brownian Surfaces Prepared through Two-Photon Polymerization: Investigation of Stem Cell Response. *ACS Nano* **2014**, *8*, 11869–11882.

(6)   Marino, A.; Barsotti, J.; De Vito, G.; Filippeschi, C.; Mazzolai, B.; Piazza, V.; Labardi, M.; Mattoli, V.; Ciofani, G. Two-Photon Lithography of 3D Nanocomposite Piezoelectric Scaffolds for Cell Stimulation. *ACS Appl. Mater. Interfaces* **2015**, *7*, 25574–25579.

(7)   Liu, X.; Gu, H.; Wang, M.; Du, X.; Gao, B.; Elbaz, A.; Sun, L.; Liao, J.; Xiao, P.; Gu, Z. 3D Printing of Bioinspired Liquid Superrepellent Structures. *Adv. Mater.* **2018**, *30*, 1800103.

(8)   Lin, Y.; Zhou, R.; Xu, J. Superhydrophobic Surfaces Based on Fractal and Hierarchical Microstructures Using Two-Photon Polymerization: Toward Flexible Superhydrophobic Films. *Adv. Mater. Interfaces* **2018**, *5*, 1–8.

(9)   Servant, A.; Qiu, F.; Mazza, M.; Kostarelos, K.; Nelson, B. J. Controlled *in vivo* Swimming of a Swarm of Bacteria-like Microrobotic Flagella. *Adv. Mater.* **2015**, *27*, 2981–2988.

(10)   Bozuyuk, U.; Yasa, O.; Yasa, I. C.; Ceylan, H.; Kizilel, S.; Sitti, M. Light-Triggered Drug Release from 3D-Printed Magnetic Chitosan Microswimmers. *ACS Nano* **2018**, *12*, 9617–9625.

(11)   Lamont, A. C.; Restaino, M. A.; Kim, M. J.; Sochol, R. D. A Facile Multi-Material Direct Laser Writing Strategy. *Lab Chip* **2019**, *19*, 2340–2345.

(12)   Mayer, F.; Richter, S.; Westhauser, J.; Blasco, E.; Barner-Kowollik, C.; Wegener, M. Multimaterial 3D Laser Microprinting Using an Integrated Microfluidic System. *Sci. Adv.* **2019**, *5*, 1–8.

(13)   Ovsianikov, A.; Viertl, J.; Chichkov, B.; Oubaha, M.; MacCraith, B.; Sakellari, I.; Giakoumaki, A.; Gray, D.; Vamvakaki, M.; Farsari, M.; Fotakis, C. Ultra-Low Shrinkage Hybrid Photosensitive Material for Two-Photon Polymerization Microfabrication. *ACS Nano* **2008**, *2*, 2257–2262.

(14)   Gansel, J. K.; Thiel, M.; Rill, M. S.; Decker, M.; Bade, K.; Saile, V.; Von Freymann, G.; Linden, S.; Wegener, M. Gold Helix Photonic Metamaterial as Broadband Circular Polarizer. *Science* **2009**, *325*, 1513–1515.

(15)   Zyla, G.; Kovalev, A.; Heisterkamp, S.; Esen, C.; Gurevich, E. L.; Gorb, S.; Ostendorf, A.

Biomimetic Structural Coloration with Tunable Degree of Angle-Independence Generated by Two-Photon Polymerization. *Opt. Mater. Express* **2019**, *9*, 2630.

(16)   Liu, Y.; Wang, H.; Ho, J.; Ng, R. C.; Ng, R. J. H.; Hall-Chen, V. H.; Koay, E. H. H.; Dong, Z.; Liu, H.; Qiu, C. W.; Greer, J. R.; Yang, J. K. W. Structural Color Three-Dimensional Printing by Shrinking Photonic Crystals. *Nat. Commun.* **2019**, *10*.

(17)   Hippler, M.; Lemma, E. D.; Bertels, S.; Blasco, E.; Barner-Kowollik, C.; Wegener, M.; Bastmeyer, M. 3D Scaffolds to Study Basic Cell Biology. *Adv. Mater.* **2019**, *31*, 1808110.

(18)   Hippler, M.; Blasco, E.; Qu, J.; Tanaka, M.; Barner-Kowollik, C.; Wegener, M.; Bastmeyer, M. Controlling the Shape of 3D Microstructures by Temperature and Light. *Nat. Commun.* **2019**, *10*, 232.

(19)   Jin, D.; Chen, Q.; Huang, T. Y.; Huang, J.; Zhang, L.; Duan, H. Four-Dimensional Direct Laser Writing of Reconfigurable Compound Micromachines. *Mater. Today* **2019**, *32*, 19–25.

(20)   Ceylan, H.; Yasa, I. C.; Yasa, O.; Tabak, A. F.; Giltinan, J.; Sitti, M. 3D-Printed Biodegradable Microswimmer for Theranostic Cargo Delivery and Release. *ACS Nano* **2019**, *13*, 3353–3362.

(21)   Tudor, A.; Delaney, C.; Zhang, H.; Thompson, A. J.; Curto, V. F.; Yang, G. Z.; Higgins, M. J.; Diamond, D.; Florea, L. Fabrication of Soft, Stimulus-Responsive Structures with Sub-Micron Resolution *via* Two-Photon Polymerization of Poly(Ionic Liquid)S. *Mater. Today* **2018**, *21*, 807–816.

(22)   Zeng, H.; Wasylczyk, P.; Parmeggiani, C.; Martella, D.; Burresi, M.; Wiersma, D. S. Light-

Fueled Microscopic Walkers. *Adv. Mater.* **2015**, *27*, 3883–3887.

(23)   Flatae, A. M.; Burresi, M.; Zeng, H.; Nocentini, S.; Wiegele, S.; Parmeggiani, C.; Kalt, H.; Wiersma, D. Optically Controlled Elastic Microcavities. *Light Sci. Appl.* **2015**, *4*, 2–6.

(24)   Chen, L.; Dong, Y.; Tang, C. Y.; Zhong, L.; Law, W. C.; Tsui, G. C. P.; Yang, Y.; Xie, X. Development of Direct-Laser-Printable Light-Powered Nanocomposites. *ACS Appl. Mater. Interfaces* **2019**, *11*, 19541–19553.

(25)   Zanotto, S.; Sgrignuoli, F.; Nocentini, S.; Martella, D.; Parmeggiani, C.; Wiersma, D. S. Multichannel Remote Polarization Control Enabled by Nanostructured Liquid Crystalline Networks. *Appl. Phys. Lett.* **2019**, *114*, 201103.

(26)   McCracken, J. M.; Tondiglia, V. P.; Auguste, A. D.; Godman, N. P.; Donovan, B. R.; Bagnall, B. N.; Fowler, H. E.; Baxter, C. M.; Matavulj, V.; Berrigan, J. D.; White, T. J. Microstructured Photopolymerization of Liquid Crystalline Elastomers in Oxygen-Rich Environments. *Adv. Funct. Mater.* **2019**, *29*, 1903761.

(27)   Yoshida, H.; Lee, C. H.; Fujii, A.; Ozaki, M. Tunable Single Photonic Defect-Mode in Cholesteric Liquid Crystals with Laser-Induced Local Modifications of Helix. *Appl. Phys. Lett.* **2006**, *89*, 231913.

(28)   Nocentini, S.; Martella, D.; Parmeggiani, C.; Wiersma, D. S. Photoresist Design for Elastomeric Light Tunable Photonic Devices. *Materials (Basel).* **2016**, *9*, 1–11.

(29)   Carlotti, M.; Mattoli, V. Functional Materials for Two-Photon Polymerization in Microfabrication. *Small.* **2019**, 15, 1902687.

(30)   Mulder, D. J.; Schenning, A. P. H. J.; Bastiaansen, C. W. M. Chiral-Nematic Liquid Crystals as One Dimensional Photonic Materials in Optical Sensors. *J. Mater. Chem. C* **2014**, *2*, 6695–6705.

(31)   Stumpel, J. E.; Broer, D. J.; Bastiaansen, C. W. M.; Schenning, A. P. H. J. Optical and Topographic Changes in Water-Responsive Patterned Cholesteric Liquid Crystalline Polymer Coatings. *Organic Photonics* **2014**, 9137, 91370U.

(32)   Moirangthem, M.; Schenning, A. P. H. J. Full Color Camouflage in a Printable Photonic Blue-Colored Polymer. *ACS Appl. Mater. Interfaces* **2018**, *10*, 4168–4172.

(33)   Yoshida, H.; Lee, C. H.; Matsuhisa, Y.; Fujii, A.; Ozaki, M. Bottom-up Fabrication of Photonic Defect Structures in Cholesteric Liquid Crystals Based on Laser-Assisted Modification of the Helix. *Adv. Mater.* **2007**, *19*, 1187–1190.

(34)   Yoshida, H. Functionalisation of Cholesteric Liquid Crystals by Direct Laser Writing. *Liq. Cryst. Today* **2012**, *21*, 3–19.

(35)   Tartan, C. C.; Salter, P. S.; Booth, M. J.; Morris, S. M.; Elston, S. J. Localised Polymer Networks in Chiral Nematic Liquid Crystals for High Speed Photonic Switching. *J. Appl. Phys.* **2016**, *119*, 183106.

(36)   van Heeswijk, E. P. A.; Kloos, J. J. H.; Grossiord, N.; Schenning, A. P. H. J. Humidity-Gated, Temperature-Responsive Photonic Infrared Reflective Broadband Coatings. *J. Mater. Chem. A* **2019**, *7*, 6113–6119.

(37)   Plamadeala, C.; Hischen, F.; Friesenecker, R.; Wollhofen, R.; Jacak, J.; Buchberger, G.; Heiss, E.; Klar, T. A.; Baumgartner, W.; Heitz, J. Bioinspired Polymer Microstructures for

Directional Transport of Oily Liquids. *R. Soc. Open Sci.* **2017**, *4*, 160849.

(38) Jisha, C. P.; Hsu, K. C.; Lin, Y.; Lin, J. H.; Jeng, C. C.; Lee, R. K. Pattern Writing in a Liquid-Crystal-Monomer Mixture Using Two-Photon Polymerization. *Pacific Rim Conf. Lasers Electro-Optics, CLEO - Tech. Dig.* **2013**, 1–2.

(39) Sherwood, T.; Young, C.; Takayesu, J.; Jen, A. K.; Dalton, L.; Chen, A. Polymer Ring Resonator Made by Two-Photon Polymerization and Vertically Coupled to a Side-Polished Optical Fiber. *Organic Photonic Materials and Devices* **2005**, 5724, 356.

(40) Tartan, C. C.; Sandford O'Neill, J. J.; Salter, P. S.; Aplinc, J.; Booth, M. J.; Ravnik, M.; Morris, S. M.; Elston, S. J. Read on Demand Images in Laser-Written Polymerizable Liquid Crystal Devices. *Adv. Opt. Mater.* **2018**, *6*, 1800515.

(41) Schafer, K. J.; Hales, J. M.; Balu, M.; Belfield, K. D.; Van Stryland, E. W.; Hagan, D. J. Two-Photon Absorption Cross-Sections of Common Photoinitiators. *J. Photochem. Photobiol. A Chem.* **2004**, *162*, 497–502.

(42) van Kuringen, H. P. C.; Leijten, Z. J. W. A.; Gelebart, A. H.; Mulder, D. J.; Portale, G.; Broer, D. J.; Schenning, A. P. H. J. Photoresponsive Nanoporous Smectic Liquid Crystalline Polymer Networks: Changing the Number of Binding Sites and Pore Dimensions in Polymer Adsorbents by Light. *Macromolecules* **2015**, *48*, 4073–4080.

(43) Zuo, B.; Wang, M.; Lin, B.-P. P.; Yang, H. Photomodulated Tricolor-Changing Artificial Flowers. *Chem. Mater.* **2018**, *30*, 8079–8088.

(44) Koepele, C. A.; Guix, M.; Bi, C.; Adam, G.; Cappelleri, D. J. 3D-Printed Microrobots with Integrated Structural Color for Identification and Tracking. *Adv. Intell. Syst.* **2020**, 1900147.

(45) Foelen, Y.; Van Der Heijden, D. A. C.; del Pozo, M.; Lub, J.; Bastiaansen, C. W. M.; Schenning, A. P. H. J. An Optical Steam Sterilization Sensor Based on a Dual-Responsive Supramolecular Cross-Linked Photonic Polymer. *ACS Appl. Mater. Interfaces* **2020**, *12*, 16896–16902.